https://doi.org/10.5194/egusphere-2026-4792
Preprint. Discussion started: 4 September 2026

Reduced Black Carbon Deposition Weakens Arctic Snow Darkening and Snowmelt Acceleration during 2046-2050

Zilu Zhang[1], Libo Zhou[2], and Meigen Zhang[2]

[1] College of Meteorology and Oceanography, National University of Defense Technology, Changsha, China

[2] Laboratory of Atmosphere Boudary Layer (LABL), Institute of Atmospheric Physics, Chinese Academy of Sciences, Beijing, China

Corresponding author: Libo Zhou (zhoulibo@mail.iap.ac.cn)

Abstract: Air-pollution mitigation can reduce Arctic black carbon (BC) deposition and thereby slow Arctic warming by weakening snow darkening and associated radiative effects. Yet the regional land-surface benefits of future BC-deposition reductions across contrasting mitigation pathways remain poorly quantified. We use Polar-WRF coupled online with the SNICAR snow-albedo scheme to isolate the effects of spatially heterogeneous BC deposition associated with low-emission (SSP1-2.6), intermediate-emission (SSP2-4.5), and high-emission (SSP5-8.5) pathways during 2046–2050. All experiments share an SSP2-4.5 large-scale meteorological background and differ only in prescribed BC deposition; they therefore quantify the BC-deposition pathway rather than the full climate response to each SSP. Relative to simulations without BC in snow, Arctic-mean spring snow albedo decreases by 16.9 %, 18.1 %, and 19.3 % under SSP1-2.6, SSP2-4.5, and SSP5-8.5, respectively. BC deposition increases surface net radiation by 1.0–1.4 W m^{-2}, spring snowmelt by 4.1–6.1 mm d^{-1}, advances snow disappearance by 6.7–7.6 days, and increases Arctic land-mean near-surface air temperature by 0.09–0.12 °C. Compared with SSP5-8.5, the 39.6 % lower BC deposition under SSP1-2.6 produces 12.4 %, 28.6 %, and 32.8 % smaller BC-induced changes in snow albedo, net radiation, and snowmelt, respectively. Responses are regionally heterogeneous: Greenland shows the strongest albedo and snowmelt responses despite relatively low deposition, whereas the European Arctic and West Siberia show stronger radiative responses, where substantial snow darkening coincides with greater incoming solar radiation. These results provide a process-based,

https://doi.org/10.5194/egusphere-2026-4792
Preprint. Discussion started: 4 September 2026

regional evaluation of the deposition-related Arctic climate benefits of mid-century mitigation pathways.

Key words: Black Carbon deposition; Arctic; snow albedo; snowmelt; mitigation pathways

1. Introduction

Air-pollution mitigation can influence both air quality and near-term Arctic climate by changing emissions of short-lived climate forcers. This linkage is especially relevant in the Arctic, where surface air temperature has increased at nearly four times the global rate since 1979 (Rantanen et al., 2022). Scenario-based assessments have shown that technically feasible reductions in short-lived climate forcers could avoid 0.2 ± 0.17 K of Arctic warming by 2050, with targeted reductions in carbonaceous particulate matter, particularly black carbon (BC), offering additional near-term climate benefits (Sand et al., 2016; Von Salzen et al., 2022). As alternative emission pathways increasingly diverge toward the mid-21st century, a central question is therefore not simply whether pollution mitigation affects Arctic warming, but through which pathways and by how much.

Pollution mitigation can affect Arctic climate through two broad response pathways: changes in atmospheric pollutant burdens and their radiative effects, and changes in aerosol deposition onto snow- and ice-covered surfaces. Most policy-oriented assessments have summarized the combined climate response in terms of Arctic-mean radiative forcing or surface temperature change, even when contributions from individual processes are estimated. For example,Von Salzen et al. (2022) projected that maximum feasible BC emission reductions could avoid 0.3 °C (0.1–0.4 °C) of Arctic warming in 2050, with approximately 0.2 °C attributed to reduced BC interactions with surface albedo. This result indicates that the surface-albedo pathway can account for a substantial share of the Arctic climate benefit from BC mitigation. However, Arctic-mean temperature and radiative metrics do not show how changes in BC deposition are translated into regional snow and land-surface responses.

Deposition-focused evaluations provide further quantitative evidence but also reveal important limitations. After correcting model biases against observations, Jiao et al. (2014) estimated an Arctic-mean radiative effect of approximately 0.17 W m^{-2} from BC in snow. Kühn et al. (2020b) projected that additional emission mitigation in Arctic Council member states could reduce Arctic BC deposition by 33.8% in 2050, but inferred the associated snow radiative

https://doi.org/10.5194/egusphere-2026-4792
Preprint. Discussion started: 4 September 2026

forcing from a linear deposition–forcing relationship rather than explicitly calculating changes in snow albedo and snow processes. Hao et al. (2023) further showed that projected declines in BC deposition could reduce the December–May radiative forcing of light-absorbing particles in Northern Hemisphere snow from 1.3 W m^{-2} in 1995–2014 to 0.49–0.65 W m^{-2} by 2081–2100. However, that study focused on hemispheric and end-of-century changes, with regional snowpack responses evaluated primarily over the Tibetan Plateau. Thus, how mid-century changes in BC deposition affect Arctic snow albedo, surface energy balance, snowmelt, and near-surface climate at the regional scale remains insufficiently quantified.

The Shared Socioeconomic Pathways provide a consistent framework for addressing this gap because they link contrasting socioeconomic and energy futures with different assumptions about air-pollution control and pollutant emissions (O’neill et al., 2014; Riahi et al., 2017). SSP1-2.6, SSP2-4.5, and SSP5-8.5 represent sustainability-oriented low-forcing, intermediate, and fossil-fuel-intensive high-forcing pathways, respectively. Their associated BC deposition fields span lower, intermediate, and higher levels of Arctic BC deposition during 2046–2050. This period captures differences that have developed after several decades of divergent energy use and emission control and is consistent with the 2050 horizon adopted in recent evaluations of Arctic pollution mitigation (Kühn et al., 2020a; Von Salzen et al., 2022). Comparing these deposition fields therefore provides a means of evaluating how different levels of emission mitigation alter the contribution of BC deposition to Arctic snow and surface climate.

Accordingly, this study quantifies how scenario-dependent BC deposition modifies Arctic snow and land-surface climate during 2046–2050. Unlike idealized sensitivity experiments that impose fixed BC concentrations in snow, the simulations apply spatially heterogeneous BC deposition fields from SSP1-2.6, SSP2-4.5, and SSP5-8.5 within Polar-WRF coupled online with the SNICAR snow-albedo scheme. All experiments use the same SSP2-4.5 large-scale meteorological background and differ only in the prescribed BC deposition. This configuration isolates surface responses attributable to differences in BC deposition rather than representing the full climate response to each SSP. The objectives are to (1) quantify differences in BC deposition and the resulting snow-albedo reduction among the three pathways; (2) determine the associated changes in surface radiation, near-surface air temperature, snowmelt rate, and snow-disappearance timing; and (3) characterize the regional heterogeneity of these responses. The

https://doi.org/10.5194/egusphere-2026-4792
Preprint. Discussion started: 4 September 2026

comparison provides a process-based, regional evaluation of the land-surface climate implications of BC-deposition changes under mid-century mitigation pathways.

2 Materials and Methods

2.1 Model configuration

This study employs the polar-optimized Weather Research and Forecasting model (Polar-WRF, version 4.1.1), a regional climate model specifically adapted for polar regions. Polar-WRF incorporates several improvements over the standard WRF model for high-latitude applications, including optimized heat transfer through snow and ice, revised surface energy balance calculations in the Noah-MP land surface model, a comprehensive representation of sea ice properties (thickness, density, and albedo), and adjustments to cloud microphysical parameters appropriate for polar conditions (Hines and Bromwich, 2008; Hines et al., 2015). The model domain (**Figure 1**) covers the entire Arctic region north of approximately 60°N using a polar stereographic projection centered at the North Pole, with a horizontal resolution of 27 km (220 × 220 grid cells) and 50 vertical levels extending from the surface to 10 hPa.

The physical parameterization schemes are selected based on prior evaluations for Arctic applications (Hines et al., 2019; Zhang et al., 2025). The Morrison-2-moment scheme (Morrison and Gettelman, 2008) is used for cloud microphysics, as it has been shown to provide the best overall performance for simulating Arctic surface radiation and cloud properties (Zhang et al., 2026). The Mellor–Yamada–Nakanishi–Niino (MYNN) level 2.5 scheme is employed for boundary layer turbulence, with the corresponding MYNN surface layer scheme (Nakanishi and Niino, 2009, 2006). The Rapid Radiative Transfer Model for General Circulation Models (RRTMG) handles both longwave and shortwave radiation (Iacono et al., 2008). The Noah-MP land surface model provides the lower boundary conditions over land (Niu et al., 2011). The Kain–Fritsch cumulus parameterization is applied on the 27 km grid (Kain, 2004).

A central feature of the modeling system is the online coupling of the Snow, Ice, and Aerosol Radiative (SNICAR) model (Flanner et al., 2021; Flanner et al., 2007) with Polar-WRF. SNICAR computes spectrally resolved snow albedo across five wavelength bands (0.2–5.0 μm) based on the two-stream radiative transfer solution of (Toon et al., 1989), explicitly accounting for the mass concentration and optical properties of light-absorbing aerosols embedded in the

https://doi.org/10.5194/egusphere-2026-4792
Preprint. Discussion started: 4 September 2026

snowpack. In the online coupling configuration, Polar-WRF provides meteorological and snow state variables to SNICAR at each radiation time step, and SNICAR returns the computed snow albedo to the Noah-Mp surface scheme. This two-way coupling ensures that BC-induced albedo changes feed back onto the surface energy balance, snowmelt, and near-surface meteorology in a physically consistent manner (Zhang et al., 2025).

2.2 Experimental Design

Four simulations are conducted to isolate the impacts of BC deposition under different emission pathways. **Table 1** summarizes the experiment configurations and the characteristics of each SSP scenario. A control simulation (CTL) without BC in snow provides the baseline against which BC effects are quantified. In the three BC experiments, BC concentrations in snow are prescribed based on deposition fluxes from the CMIP6 NorESM2-LM model under SSP1-2.6, SSP2-4.5, and SSP5-8.5, respectively. All BC experiments share the same meteorological initial and boundary conditions and differ only in the BC loading, thereby isolating the radiative and surface energy impacts of BC deposition under each emission pathway. Each simulation covers the period 2046–2050, with the first month treated as spin-up and excluded from analysis.

Table 1 Summary of experimental design and SSP scenario characteristics.

Experiment	SSP scenario	Forcing level	Socioeconomic narrative
CTL	—	—	—
SEN_ssp126	SSP1-2.6	Low (2.6 W m^{-2} by 2100)	Sustainability-focused pathway; low population growth, high education, rapid technological change, strong environmental policies
SEN_ssp245	SSP2-4.5	Medium (4.5 W m^{-2} by 2100)	Intermediate pathway; social, economic, and technological trends follow historical patterns without major deviations
SEN_ssp585	SSP5-8.5	High (8.5 W m^{-2} by 2100)	Fossil-fuel-intensive pathway; rapid economic

https://doi.org/10.5194/egusphere-2026-4792
Preprint. Discussion started: 4 September 2026

	growth driven by carbon-intensive energy, high anthropogenic emissions

2.3 Data

The meteorological initial and lateral boundary conditions for all simulations are derived from a bias-corrected CMIP6 dataset generated using the high-resolution MPI-ESM1-2-HR model output under the SSP2-4.5 scenario (Xu et al., 2021). This dataset provides 6-hourly fields of geopotential height, temperature, zonal and meridional wind, specific humidity, and surface pressure at a horizontal resolution of 1.25° × 1.25° across 14 pressure levels, with the bias correction performed against the ERA5 reanalysis for the historical period (1979–2014) using the ensemble mean of 18 CMIP6 models. The use of a common SSP2-4.5 climate background for all experiments ensures that differences in simulated BC impacts are attributable solely to the prescribed BC deposition fluxes rather than to differences in the background climate state. Initial snow conditions are obtained from the NCEP GDAS/FNL dataset at 0.25° resolution.

The BC deposition fluxes used to prescribe snow BC concentrations are derived from the Norwegian Earth System Model version 2 (NorESM2-LM), which has been evaluated as performing well in simulating present-day Arctic BC concentrations and their radiative effects (Chen et al., 2024). Monthly BC deposition fluxes for the three SSP scenarios are obtained for the 2046–2050 period. The BC mass concentration in each snow layer is calculated by integrating the deposition flux over the snow accumulation period and distributing it according to the snow water equivalent of each layer, following (Zhang et al., 2025).

All results are analyzed over the Arctic land area, defined as model grid cells north of 60°N with a land fraction exceeding 50 %. For regional analysis, the domain is divided into five sub-regions following the classification employed in previous Arctic BC studies (Dou and Xiao, 2016; Zhang et al., 2024): Greenland, North America, the European Arctic, West Siberia, and East Siberia. BC-induced changes are calculated as the difference between each BC experiment and the CTL simulation. All reported values represent temporal averages over the 2046–2050 period for the spring melt season (March–May), when solar radiation is sufficient for the snow albedo feedback to operate and BC deposition has the strongest impact on snowmelt.

https://doi.org/10.5194/egusphere-2026-4792
Preprint. Discussion started: 4 September 2026

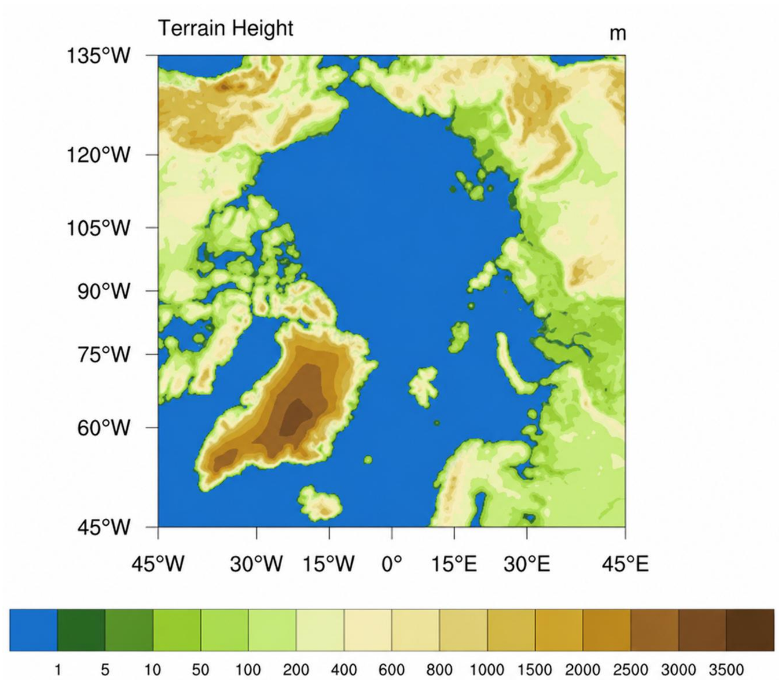

Figure 1. Polar-WRF domains and terrain height.

3 Results

3.1 BC deposition fluxes under three SSP scenarios

To quantitatively assess the impacts of future BC deposition on Arctic land surface processes, a prerequisite is understanding the magnitude and spatial distribution of BC deposition fluxes themselves. As the primary forcing agent in the snow darkening chain, BC deposition flux directly determines the amount of light‐ absorbing impurities introduced into the snowpack, thereby setting the upper bound for subsequent albedo reduction, surface energy perturbations, and snowmelt acceleration. This section therefore first examines the BC deposition fluxes across the Arctic during 2046–2050 under the three SSP scenarios.

Figure 2 presents the spatial distribution and regional averages of BC deposition fluxes over the Arctic during 2046–2050 under the three SSP scenarios. A pronounced scenario‐dependent increase in deposition flux is evident, with the domain-averaged values rising from 15.4 ± 7.9 mg m^{-2} d^{-1} in SSP1-2.6 to 18.4 ± 8.7 mg m^{-2} d^{-1} in SSP2-4.5 and 25.5 ± 12.1 mg m^{-2} d^{-1} in SSP5-8.5 (**Figure 2d**). The difference between the highest and lowest emission pathways thus

https://doi.org/10.5194/egusphere-2026-4792
Preprint. Discussion started: 4 September 2026

reaches a factor of 1.7, reflecting the strong sensitivity of Arctic BC burden to anthropogenic emission trajectories.

Despite these magnitude differences, the spatial pattern of BC deposition remains remarkably consistent across the three scenarios (**Figure 2a–c**). The highest deposition fluxes occur over West Siberia, followed by East Siberia, the European Arctic, North America, and Greenland. This ordering is in good agreement with the geographic distribution inferred from historical snow BC observations (Dou and Xiao, 2016; Zhang et al., 2024), which indicates that the relative importance of source regions and transport pathways persists under future climate conditions. West Siberia and East Siberia are located close to major industrial and biomass-burning emission sources in Eurasia, whereas Greenland receives considerably lower BC fluxes due to its remote location and effective scavenging during long-range transport (Qi and Wang, 2019).

The regional boxplots (**Figure 2d)** further reveal that the inter-scenario differences are largest in regions with high absolute deposition, particularly West and East Siberia, where the SSP5-8.5 fluxes exceed those under SSP1-2.6 by more than 60 %. In contrast, over Greenland the relative increase is smaller in absolute terms, consistent with its overall low deposition regime. These scenario-dependent BC fluxes serve as the primary input for the subsequent simulations of snow albedo reduction and surface energy balance changes (Sections 3.2 and 3.3).

https://doi.org/10.5194/egusphere-2026-4792
Preprint. Discussion started: 4 September 2026

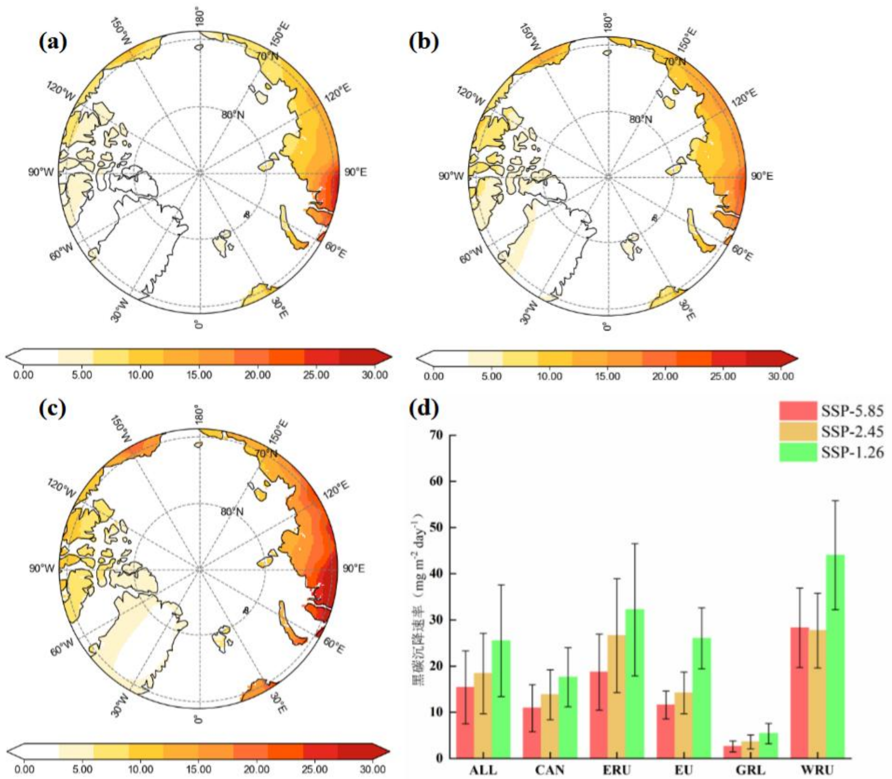

Figure 2.Spatial distribution of BC deposition flux (mg m^{-2} d^{-1}) during 2046–2050 under (a) SSP1-2.6, (b) SSP2-4.5, and (c) SSP5-8.5. Panel (d) shows regiona-average BC deposition fluxes for the five Arctic sub-regions defined in the inset map; boxes indicate the 25th–75th percentiles, whiskers the 5th–95th percentiles, and solid lines the medians. The sub-regions are: Greenland (GR), North America (NA), European Arctic (EA), West Siberia (WS), and East Siberia (ES).

3.2 Snow Albedo Reduction and Its Spatial Drivers

The BC deposition fluxes quantified in Section 3.1 directly determine the loading of light-absorbing impurities within the snowpack, thereby driving a reduction in snow albedo. **Figure 3** presents the spatial distribution of BC-induced snow albedo changes during 2046–2050 under the three SSP scenarios. Across all scenarios, BC deposition leads to widespread darkening of the Arctic snow surface, with domain-averaged albedo reductions reaching 16.9 ± 10.1% (SSP1-2.6), 18.1 ± 10.6% (SSP2-4.5), and 19.3 ± 10.8% (SSP5-8.5) (**Figure 3d; Table 2**). The progressive

https://doi.org/10.5194/egusphere-2026-4792
Preprint. Discussion started: 4 September 2026

increase from the low to high emission pathway directly reflects the scenario-dependent enhancement in BC deposition flux (Section 3.1)..

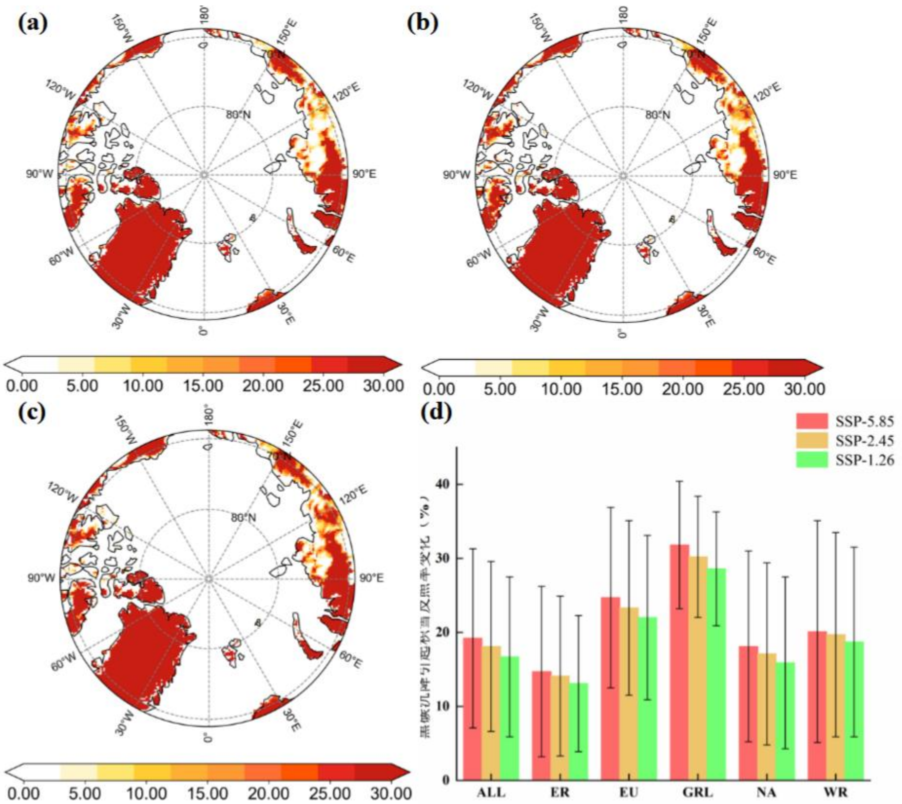

Figure 3. Spatial distribution of BC-induced snow albedo reduction (%) during 2046−2050 under (a) SSP1-2.6, (b) SSP2-4.5, and (c) SSP5-8.5. Panel (d) shows regional-average albedo reductions for the five Arctic sub-regions; boxes indicate the 25th−75th percentiles, whiskers the 5th−95th percentiles, and solid lines the medians.

Despite the differences in magnitude, the spatial pattern of albedo reduction is remarkably consistent across the three scenarios (**Figure. 3a–c**). The largest reductions consistently occur over Greenland, where the regional mean exceeds 27% under all three SSPs, reaching 32.1 ± 11.5% in SSP5-8.5 (**Table 2**). The European Arctic and West Siberia also exhibit pronounced albedo decreases, with reductions of 23.8–25.4% and 18.7–20.7%, respectively, across the three scenarios. In contrast, East Siberia consistently shows the weakest response, with albedo reductions of only 13.3–15.3%.

https://doi.org/10.5194/egusphere-2026-4792
Preprint. Discussion started: 4 September 2026

A notable feature of this spatial pattern is that it does not simply follow the distribution of BC deposition flux. Greenland receives the lowest BC deposition flux among all sub-regions (**Figure 3**), yet it exhibits the strongest albedo reduction. Conversely, West Siberia, which receives the highest BC flux, shows a smaller albedo reduction than both Greenland and the European Arctic. This apparent paradox is resolved by considering the strong modulating role of snow depth. As summarized in **Table 2**, Greenland is characterized by deep, persistent snow cover (regional mean depth of 1.65 ± 1.20 m), which increases the optical path length within the snow column and enhances the probability of photon absorption by BC particles before they can escape back to the surface. The European Arctic also possesses relatively deep snow (1.10 ± 0.8 m), which, combined with its moderately high BC deposition, produces the second‐ largest albedo reduction. West Siberia and North America, with intermediate snow depths (0.79 ± 0.60 m and 0.69 ± 0.42 m, respectively), fall between these two extremes. At the opposite end, East Siberia exhibits both the shallowest snow cover (0.25 ± 0.13 m) and the lowest BC deposition flux among the Eurasian regions, resulting in the weakest albedo response. In such shallow‐snow regimes, photons have a high probability of reaching and being reflected by the underlying ground before encountering a significant number of BC particles, thereby limiting the effective albedo reduction.

Table 2. Regional-average BC-induced snow albedo reduction and snow depth for the three SSP scenarios. Values in parentheses are ±1 standard deviation.

Region	Snow depth (m)	Snow albedo reduction in SSP1-2.6 (%)	Snow albedo reduction in SSP2-4.5 (%)	Snow albedo reduction in SSP5-8.5 (%)
Greenland	1.65 (1.2)	27.2 (12.1)	29.8 (12.4)	32.1 (11.5)
West Siberia	0.79 (0.60)	18.7 (13.6)	19.8 (13.9)	20.7 (15.4)
East Siberia	0.25 (0.13)	13.3 (10.4)	14.1 (10.6)	15.3 (11.5)
North America	0.69 (0.42)	16.2 (12.4)	18,2 (12.9)	18,7 (13.3)
European Arctic	1.1 (0.86)	23.8 (9.8%)	25.0 (10.2)	25.4 (11.8)

The comparison between the European Arctic and West Siberia offers valuable insights: although West Siberia experiences greater black carbon (BC) deposition (**Figure 2**), the

https://doi.org/10.5194/egusphere-2026-4792
Preprint. Discussion started: 4 September 2026

European Arctic exhibits a more pronounced reduction in albedo due to its deeper snowpack, which enhances the radiative impact of a given BC concentration. This observation aligns with the sensitivity analyses conducted by Zhang et al. (2025), who found that, for equivalent BC levels, deeper snowpacks consistently intensify albedo reduction until reaching optical saturation. The current study further confirms that this mechanism remains robust across all three Shared Socioeconomic Pathway (SSP) scenarios, indicating that the combined distribution of BC deposition flux and snow depth,rather than either variable independently determines the regions experiencing the most significant albedo decreases. While increased BC deposition under higher-emission scenarios amplifies the overall magnitude of albedo reduction, it does not substantially alter the spatial distribution pattern (**Figure 3**). A critical implication of these findings is that areas characterized by deep and persistent snow cover, such as the Greenland Ice Sheet and the European Arctic, will continue to be highly vulnerable to BC-induced surface darkening, even in the context of stringent emission reduction efforts.

In summary, the BC-induced snow albedo reduction over the Arctic is governed by the joint influence of BC deposition flux and snow depth. The BC deposition flux determines the overall magnitude of the reduction and its sensitivity to emission scenarios, while snow depth dictates the spatial pattern and identifies which regions are most susceptible to BC-induced darkening. This mechanistic understanding provides the basis for interpreting the surface radiation and energy budget perturbations discussed in the following section.

3.3 Changes in Surface Energy Balance

The snow albedo reduction documented in Section 3.2 directly modifies the surface radiative budget by enhancing the absorption of incoming solar radiation. **Figure 4** presents the spatial distribution of BC-induced changes in net shortwave radiation (ΔSWnet) at the surface during 2046-2050 under the three SSP scenarios.

The BC-induced albedo reduction leads to a widespread increase in surface-absorbed shortwave radiation across the Arctic (**Figure 4a–c**). The domain-averaged ΔSWnet rises from 1.3 ± 1.2 W m^{-2} in SSP1-2.6 to 1.5 ± 1.3 W m^{-2} in SSP2-4.5 and 1.8 ± 1.5 W m^{-2} in SSP5-8.5, mirroring the scenario-dependent progression of albedo reduction. The spatial distribution of ΔSWnet, however, does not simply replicate that of albedo reduction. The largest shortwave gains occur over the European Arctic, where ΔSWnet reaches 2.2 ± 1.1 W m^{-2} (SSP5-8.5),

https://doi.org/10.5194/egusphere-2026-4792
Preprint. Discussion started: 4 September 2026

followed by West Siberia (2.0 ± 1.6 W m^{-2}) and East Siberia (1.9 ± 1.4 W m^{-2}). Greenland, despite exhibiting the strongest albedo reduction, shows a comparatively modest ΔSWnet of 1.4 ± 1.3 W m^{-2} under SSP5-8.5. This apparent discrepancy arises from the latitudinal dependence of incoming solar radiation: the European Arctic and Siberian regions, situated at lower latitudes than Greenland, receive higher insolation during the spring melt season. Since ΔSWnet is the product of albedo reduction and incident solar flux, regions with both substantial darkening and strong insolation experience the largest absolute shortwave gains.

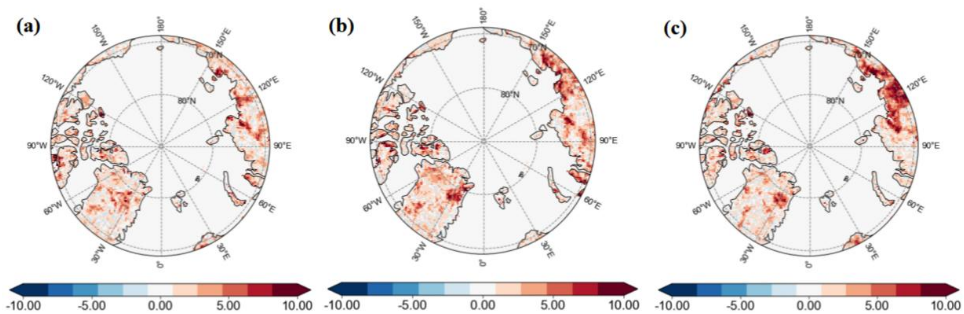

Figure 4. Spatial distribution of BC-induced changes in net surface shortwave radiation (W m^{-2}, positive downward) during 2046–2050 under (a) SSP1-2.6, (b) SSP2-4.5, and (c) SSP5-8.5.

This apparent discrepancy arises from the latitudinal dependence of incoming solar radiation: the European Arctic and Siberian regions, situated at lower latitudes than Greenland, receive higher insolation during the spring melt season. Since ΔSWnet scales with both the magnitude of albedo reduction and the incident solar flux, regions combining substantial darkening with strong insolation experience the largest absolute shortwave gains, whereas Greenland's shortwave enhancement is constrained by its high-latitude location.

The surface longwave response, shown in **Figure 5**, is more complex and spatially heterogeneous. In most regions, the enhanced shortwave absorption warms the surface, which in turn increases the upward longwave emission, producing a net longwave loss at the surface. However, the BC-induced changes in near-surface atmospheric temperature and humidity (discussed in Section 3.5) simultaneously enhance the downward longwave flux, partially compensating for the increased upward emission. The net longwave effect therefore reflects a regional balance between these competing processes (**Figure 6b**). Under SSP5-8.5, West Siberia experiences a modest net longwave gain (0.6 ± 0.9 W W m^{-2}, where enhanced atmospheric

https://doi.org/10.5194/egusphere-2026-4792
Preprint. Discussion started: 4 September 2026

back-radiation outweighs the surface emission increase. In contrast, Greenland and East Siberia exhibit a net longwave loss (−0.2 ± 0.5 W m^{-2} and −0.2 ± 0.8 W m^{-2}, respectively), indicating that surface warming dominates the longwave response in these regions. Under the lower-emission scenarios, the net longwave effect tends toward more negative values across all regions, reflecting the weaker atmospheric feedback at reduced BC loadings.

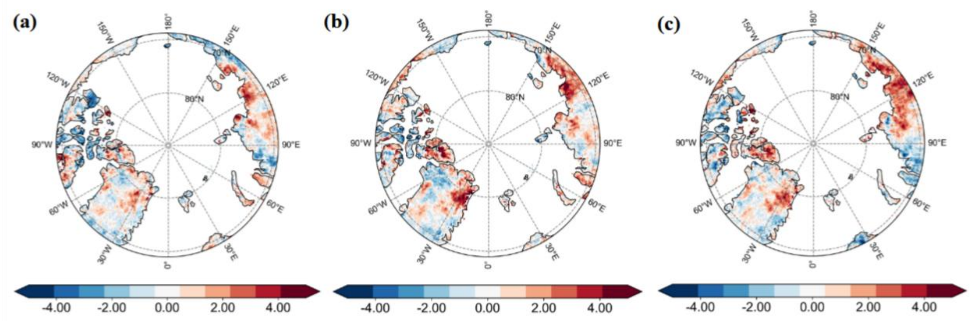

Figure 5. Spatial distribution of BC-induced changes in net surface longwave radiation (W m^{-2}, positive downward) during 2046–2050 under (a) SSP1-2.6, (b) SSP2-4.5, and (c) SSP5-8.5.

The net surface radiation change (ΔRnet = ΔSWnet + ΔLWnet) integrates these competing shortwave and longwave responses. Under SSP5-8.5 and SSP2-4.5, the domain-averaged ΔRnet reaches approximately 1.4 W m^{-2}, while SSP1-2.6 yields a smaller net increase of 1.0 ± 0.8 W m^{-2}. The regional distribution (Fig. 6a) reveals that the largest net radiation gains occur over the European Arctic (2.4 ± 1.3 W m^{-2} under SSP5-8.5), consistent with this region's combination of strong shortwave enhancement and weak longwave compensation. Greenland, where the large shortwave gain is substantially offset by enhanced longwave cooling, exhibits a more moderate net radiation increase (1.2 ± 1.0 W m^{-2}). West Siberia, despite receiving the highest BC deposition flux (Section 3.1), shows the second-largest net radiation gain (2.1–2.6 W m^{-2} across scenarios), benefiting from both substantial albedo reduction and relatively high insolation. The modest difference in domain-averaged ΔRnet between SSP5-8.5 and SSP2-4.5, despite their differing BC loadings, reflects the stronger longwave compensation under the warmer SSP5-8.5 conditions, which partially cancels the additional shortwave gain.

https://doi.org/10.5194/egusphere-2026-4792
Preprint. Discussion started: 4 September 2026

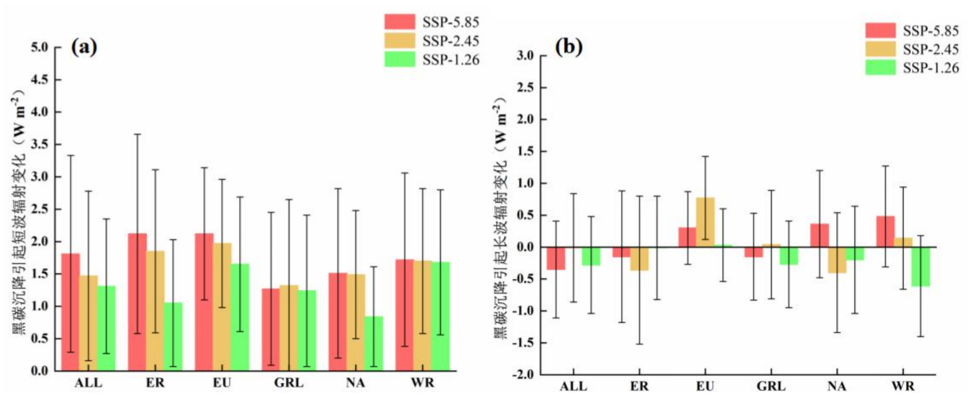

Figure 6. Regional-average BC-induced changes in (a) net shortwave radiation and (b) net longwave radiation (W m^{-2}, positive downward) for the five Arctic sub-regions under the three SSP scenarios. Boxes indicate the 25th–75th percentiles, whiskers the 5th–95th percentiles, and solid lines the medians.

The partitioning of the net radiation increment among surface energy budget components is examined in **Figure 7b.** Across all scenarios and regions, the BC-induced net radiation increase is primarily balanced by enhanced sensible heat flux and snowmelt energy consumption. Under SSP5-8.5, sensible heat flux increases by 0.5–2.1 W m^{-2} depending on region, accounting for approximately 40–60% of the net radiation gain. The energy consumed by accelerated snowmelt represents the second-largest sink, particularly over Greenland and West Siberia where deep snowpacks support sustained melt. Latent heat flux changes are comparatively small (0.1–0.9 W m^{-2}), consistent with the limited availability of liquid water for evaporation during the spring melt period when much of the surface remains snow-covered. Ground heat flux changes are negligible in most regions, as the thermal insulation of the overlying snowpack limits the downward transmission of the radiative perturbation.

A notable regional contrast emerges between Greenland and the other sub-regions. Over Greenland, a larger fraction of the net radiation increment is consumed by snowmelt rather than transferred to the atmosphere as sensible heat, reflecting the vast heat capacity of the deep ice sheet snowpack. In contrast, over the Siberian and North American regions, sensible heat flux dominates the energy partitioning, implying stronger surface-atmosphere thermal coupling. This contrast has important implications for the atmospheric response to BC deposition: regions

https://doi.org/10.5194/egusphere-2026-4792
Preprint. Discussion started: 4 September 2026

where sensible heat dominates will experience more pronounced near-surface warming and boundary-layer modifications, as discussed in Section 3.5.

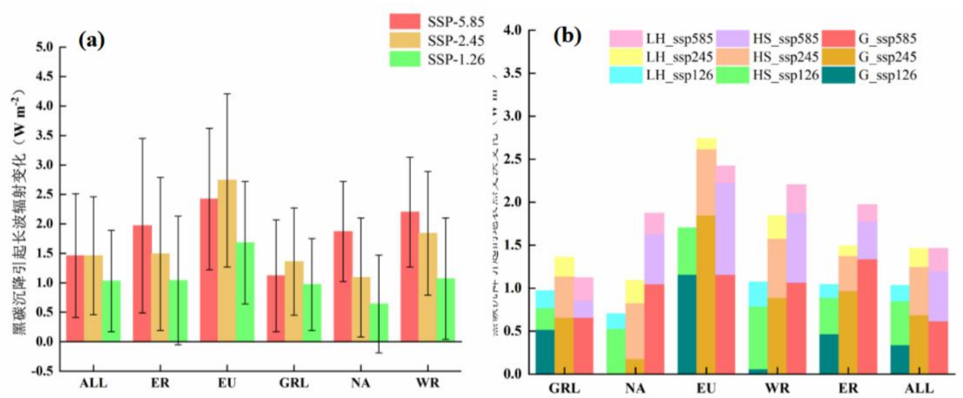

Figure 7. (a) Regional-average BC-induced changes in net surface radiation (W m⁻², positive downward) for the five Arctic sub-regions under the three SSP scenarios. Boxes indicate the 25th–75th percentiles, whiskers the 5th–95th percentiles, and solid lines the medians. (b) BC-induced surface energy budget changes (W m⁻²) by region under the three SSP scenarios. Components shown: net shortwave radiation (ΔSWnet), net longwave radiation (ΔLWnet), sensible heat flux (ΔSH), latent heat flux (ΔLH), and ground heat flux (ΔG). Positive values indicate energy gain by the surface (for radiative fluxes) or energy transfer from the surface to the atmosphere (for turbulent fluxes).

3.4 Snowmelt Acceleration and Snow Cover Change

The BC-induced snow albedo reduction and the resulting surface radiative perturbation documented in Sections 3.2 and 3.3 directly accelerate snowmelt and alter the timing of snow disappearance over the Arctic land surface. **Figure 8** presents the spatial distribution of BC-induced changes in snowmelt rate during 2046–2050 under the three SSP scenarios, and Figure 8 shows the regional statistics of snowmelt enhancement and the corresponding advance in snow disappearance timing.

The BC deposition drives a widespread acceleration of snowmelt across the Arctic (**Figure 8a–c**). The domain-averaged snowmelt rate increases by 4.1 ± 3.4 mm d^{-1}under SSP1-2.6, strengthening to 5.6 ± 4.9 mm d^{-1}under SSP2-4.5 and 6.1 ± 4.9 mm d^{-1}under SSP5-8.5, a nearly 50 % enhancement from the lowest to the highest emission pathway. The spatial pattern of

https://doi.org/10.5194/egusphere-2026-4792
Preprint. Discussion started: 4 September 2026

snowmelt enhancement closely follows that of net shortwave radiation increase (Section 3.3), with the largest values concentrated over northern Greenland, Baffin Island, and West Siberia (**Figure 9a**). Greenland shows the largest absolute snowmelt increase among all regions, with regional means of 7.1 ± 5.4 mm d^{-1}(SSP1-2.6), 10.1 ± 7.9 mm d^{-1} (SSP2-4.5), and 9.2 ± 7.0 mm d^{-1}(SSP5-8.5), consistent with its maximal albedo reduction. West Siberia follows with the secondlargest snowmelt enhancement, benefiting from both strong shortwave gain and its moderately deep snowpack. The European Arctic, despite showing the largest net radiation increase, exhibits a relatively smaller snowmelt response (1.9–3.7 mm d^{-1}), likely because its shallower snow cover limits the total meltwater production even under enhanced energy input.

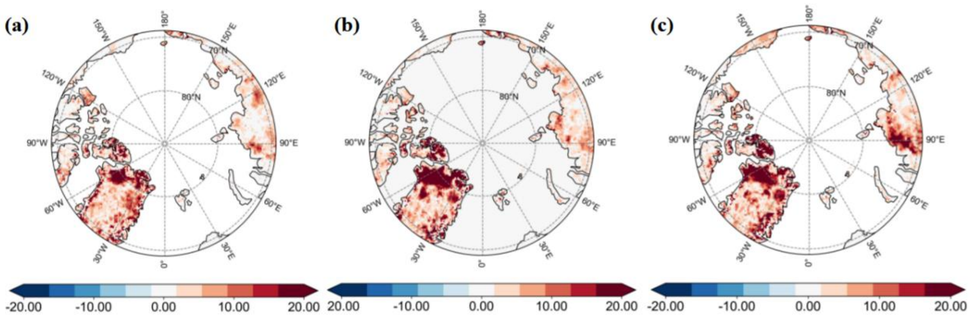

Figure 8. Spatial distribution of BC-induced changes in snowmelt rate (mm d^{-1}) during 2046–2050 under (a) SSP1-2.6, (b) SSP2-4.5, and (c) SSP5-8.5.

A more ecologically and climatically consequential metric than the melt rate itself is the advance in the timing of complete snow disappearance. Figure 8b shows the BC-induced shift in the snow-free date across the five sub-regions. The domain-averaged snow disappearance advances by 6.7 ± 3.8 days under SSP1-2.6, extending to 7.2 ± 3.2 days under SSP2-4.5 and 7.6 ± 3.5 days under SSP5-8.5. Regionally, the strongest advances occur over Greenland (up to 10.1 days under SSP5-8.5), northern Baffin Island, and West Siberia (up to 7–8 days), whereas the European Arctic shows a more modest advance of 3.7 days. The inter-scenario differences in snow disappearance timing (approximately 1 day between SSP1-2.6 and SSP5-8.5 in the domain average) are smaller than those for deposition flux or radiative forcing, because snowmelt timing is also strongly controlled by the background meteorological conditions, which are held constant across the three scenarios in experimental design (Section 2.3).

The ecological significance of earlier snow disappearance extends well beyond the immediate melt period. A 7–10 day advance in snow-free conditions exposes the underlying

https://doi.org/10.5194/egusphere-2026-4792
Preprint. Discussion started: 4 September 2026

tundra and soil surfaces to solar radiation earlier in the spring, lengthening the growing season and enhancing surface warming through the albedo feedback (Chapin et al., 2005)(Chapin et al., 2005). Earlier snowmelt also alters the timing of soil thaw, modifies the seasonality of surface hydrological processes, and can promote permafrost degradation (Bokhorst et al., 2016). These cascading impacts are particularly relevant for the climatically sensitive regions identified as northern Greenland, Baffin Island, and West Siberia, where the combination of deep snow, strong BC-induced darkening, and substantial melt acceleration produces the most pronounced changes in snow cover duration.

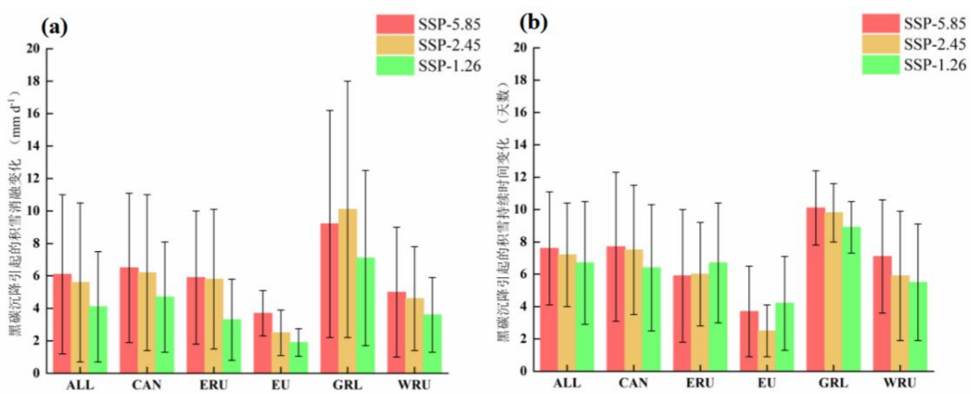

Figure 9. Regional statistics of BC-induced snowmelt changes during 2046–2050 under the three SSP scenarios. (a) Snowmelt rate increase (mm d^{-1}). (b) Advance in snow disappearance timing (days). Boxes indicate the 25th-75th percentiles, whiskers the 5th–95th percentiles, and solid lines the medians.

3.5 Near-Surface Meteorological and Cloud Responses

Beyond the direct surface radiative and snowmelt impacts, BC deposition also modifies near-surface meteorology, atmospheric vertical structure, and cloud microphysical properties through land–atmosphere feedbacks. **Figure 10** presents the spatial distribution of BC-induced changes in 2-m air temperature, specific humidity, and 10-m wind speed under the three SSP scenarios, with each row corresponding to one scenario.

The enhanced surface shortwave absorption and subsequent snowmelt drive a widespread near-surface warming over the Arctic land areas. The 2-m temperature increase scales with emission forcing, with domain-averaged values of 0.09 ± 0.06 °C (SSP1-2.6; **Figure 10a1**), 0.10 ± 0.08 °C (SSP2-4.5; **Figure 10b1**), and 0.12 ± 0.07 °C (SSP5-8.5; **Figure 10c1**). The

https://doi.org/10.5194/egusphere-2026-4792
Preprint. Discussion started: 4 September 2026

warming is most pronounced over Baffin Island, West Siberia, and northern Greenland, where local temperature increases exceed 1 °C under SSP5-8.5, consistent with the regions of strongest snow albedo reduction and sensible heat flux enhancement identified in Sections 3.2 and 3.3. The 2-m specific humidity exhibits a similar spatial pattern but with more modest magnitudes, increasing by up to 0.3 g kg^{-1} under SSP5-8.5 over the same regions (**Figure 10c2**), reflecting enhanced evaporation from the warming surface and accelerated snowmelt. Changes in 10-m wind speed are spatially heterogeneous and generally small, remaining within ±0.4 m s^{-1} across all scenarios (**Figure 10a3–c3**), with localized increases over Greenland and West Siberia and decreases over East Siberia, likely reflecting regionally specific modifications to surface roughness and boundary-layer stability induced by snow cover changes.

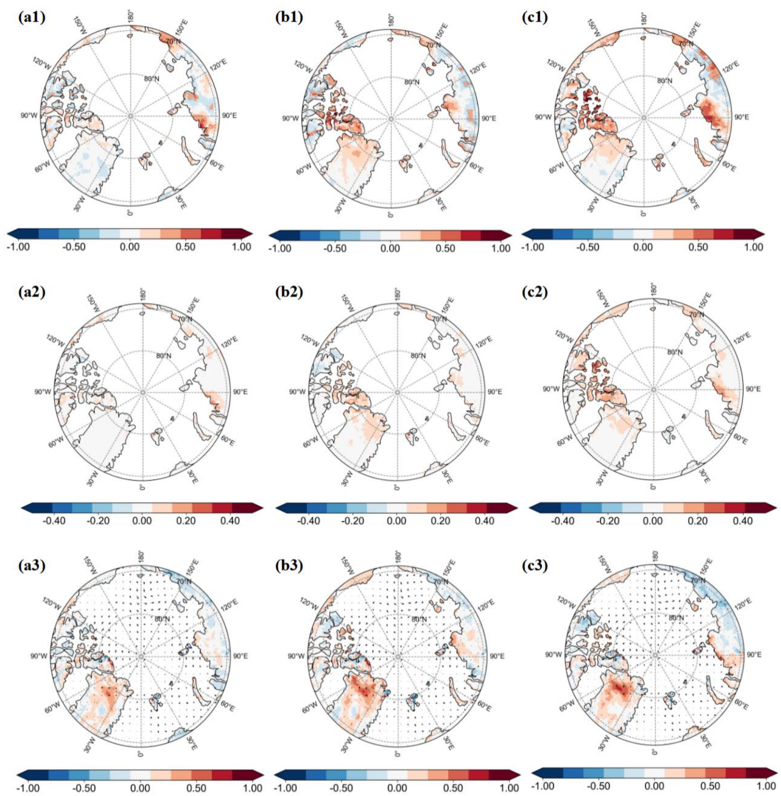

Figure 10. Spatial distribution of BC-induced changes in 2-m air temperature (°C), 2-m specific humidity (g kg^{-1}), and 10-m wind speed (m s^{-1}) during 2046–2050 under (a1–a3) SSP1-2.6, (b1–b3) SSP2-4.5, and (c1–c3) SSP5-8.5.

https://doi.org/10.5194/egusphere-2026-4792
Preprint. Discussion started: 4 September 2026

The atmospheric response to BC deposition extends well above the surface. The longitude-height cross-sections of temperature and specific humidity changes under SSP5-8.5 (**Figure 11**) reveal that significant warming penetrates to the upper troposphere (>7000 m) over the 50°W–50°E sector, with magnitudes exceeding 0.5 °C in the mid-to-upper troposphere. The specific humidity response shows a similar vertical structure but is confined to lower magnitudes (<0.15 g kg^{-1}). The deep vertical penetration of the thermal signal suggests that BC-induced surface perturbations can influence atmospheric stability and circulation beyond the boundary layer, likely through enhanced vertical mixing driven by increased sensible heat flux in the tundra regions (Section 3.3).

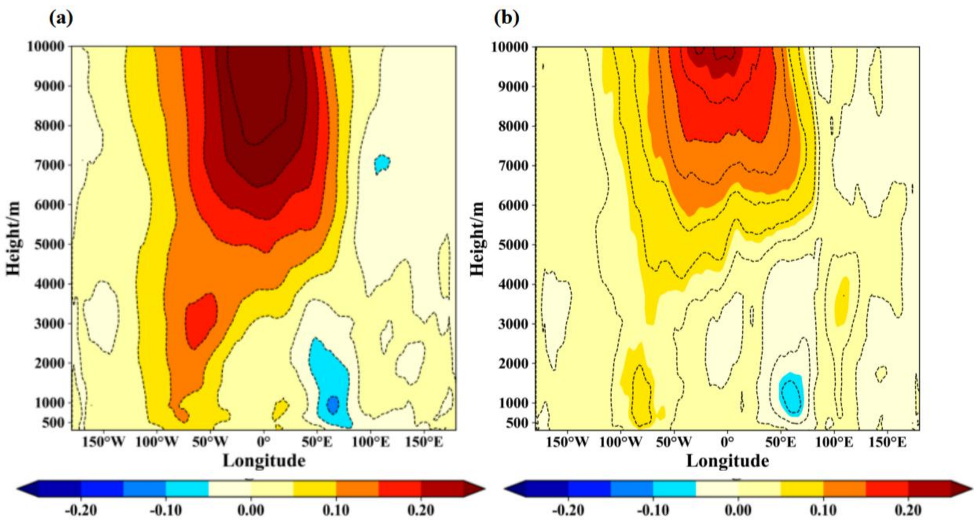

Figure 11. Longitude-height cross-sections (averaged over 65°N–90°N) of BC-induced changes in (a) air temperature (°C) and (b) specific humidity (g kg^{-1}) under SSP5-8.5 during 2046–2050.

An important and previously underappreciated consequence of these atmospheric changes is the modification of cloud microphysical properties. **Figure 12** presents the BC-induced changes in cloud liquid water fraction under the three SSP scenarios. While changes in total cloud cover are minor and spatially incoherent, the cloud liquid water fraction exhibits a consistent and scenario-dependent increase over the Arctic. Under SSP5-8.5, the liquid water fraction increases by more than 0.2 locally over Greenland, Baffin Island, and West Siberia (**Figure 12c**), regions that coincide with the strongest near-surface warming and moisture increases (**Figure 10**). The

https://doi.org/10.5194/egusphere-2026-4792
Preprint. Discussion started: 4 September 2026

domain-averaged increase is more modest but systematically intensifies from SSP1-2.6 to SSP5-8.5.

This increase in cloud liquid water fraction represents an indirect pathway through which BC deposition may influence the Arctic climate system: surface warming and enhanced evaporation promote a shift from ice-phase to liquid-phase cloud particles in mixed-phase clouds, which in turn modifies cloud radiative properties, liquid droplets are more effective shortwave reflectors and longwave emitters than ice crystals, potentially feeding back onto the surface energy balance. While the magnitude of this cloud adjustment is relatively small in the domain average, its concentration in the climatically sensitive regions of Greenland and the Siberian Arctic warrants further investigation with higher-resolution, convection-permitting simulations.

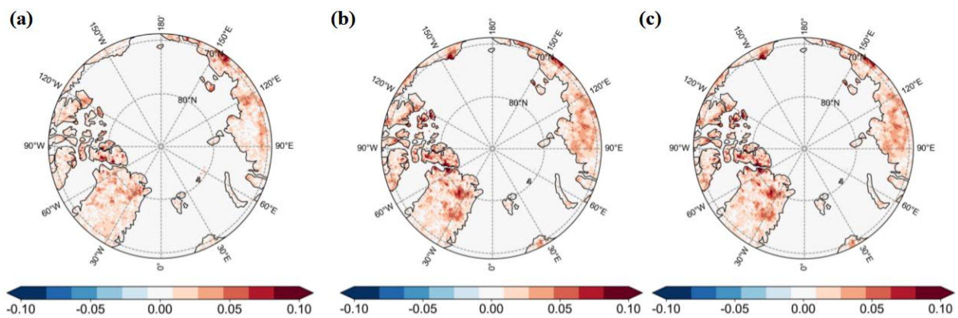

Figure 12. Spatial distribution of BC-induced changes in cloud liquid water fraction during 2046–2050 under (a) SSP1-2.6, (b) SSP2-4.5, and (c) SSP5-8.5.

3.6 Discussion

Table 3 summarizes the scenario-dependent BC-induced responses. Across the experiments, larger BC deposition is associated with stronger snow darkening, greater surface net radiation, and faster spring snowmelt. The response magnitude, however, varies among individual metrics and regions because the deposition signal is modified by the evolving snow state and surface energy balance.

The experiments isolate a coherent deposition-driven response across the Arctic land surface: greater BC loading produces larger snow darkening, increased surface net radiation, and faster spring melt. The contrast between SSP1-2.6 and SSP5-8.5 is especially informative

https://doi.org/10.5194/egusphere-2026-4792
Preprint. Discussion started: 4 September 2026

because BC deposition is about 65 % higher in the latter, whereas the corresponding BC-induced changes in snow albedo, net radiation, and snowmelt are 14 %, 40 %, and 49 % larger, respectively. The different scaling among these variables shows that deposition does not propagate linearly through the snow–energy-balance system. Snow state, solar input, melt timing, and the partitioning of additional energy between melt and turbulent fluxes all regulate the final response.

Table 3. Summary of BC-induced changes in Arctic land surface processes during 2046–2050 under three SSP scenarios.

Variable	SSP1-2.6	SSP2-4.5	SSP5-8.5	Change (SSP5-8.5 vs SSP1-2.6)
BC deposition (mg m^{-2} d^{-1})	15.4	18.4	25/5	↑ 65%
Snow albedo reduction (%)	16.9	18.1	19.3	↑ 14%
Net shortwave radiation increase (W m^{-2})	1.3	1.5	1.8	↑ 38%
Net radiation increase (W m^{-2})	1.0	1.4	1.4	↑ 40%
Snowmelt increase (mm d^{-1})	4.1	5.6	6.1	↑ 49%
Snow disappearance advance (days)	6.7	7.2	7/6	↑ 13%
Maximum local 2-m warming (°C)	~0.3	~0.7	>1.0	Significant
Increase in cloud liquid water fraction	<0.05	~0.10	>0.2	Significant

Note: Values represent domain-averaged results for the Arctic land area, except for maximum local warming and cloud liquid water fraction increase, which are reported as local maxima. Percentage changes are calculated as (SSP5-8.5 – SSP1-2.6) / SSP1-2.6 × 100%.

https://doi.org/10.5194/egusphere-2026-4792
Preprint. Discussion started: 4 September 2026

The regional patterns further show that the deposition map alone is not a map of Arctic vulnerability to BC. Greenland receives relatively low BC deposition but exhibits the strongest snow-albedo and snowmelt responses because its deep, persistent snow cover maintains an optically important snow surface through the spring melt season. In contrast, the European Arctic and West Siberia exhibit stronger surface radiative responses where appreciable snow darkening coincides with larger incoming solar radiation. This distinction is important for interpreting mitigation benefits: the largest reduction in deposition need not occur where the largest reduction in snowmelt or surface energy absorption is realized.

The analysis extends deposition-focused studies that estimated snow radiative effects from bulk deposition–forcing relationships or emphasized hemispheric, end-of-century changes (Jiao et al., 2014; Chen et al., 2024; Hao et al., 2023). It also complements the earlier idealized sensitivity analysis of snow darkening in Polar-WRF (Zhang et al., 2025). Here, spatially heterogeneous and scenario-specific deposition fields are translated through the online snow-albedo coupling into regional changes in snow albedo, surface energy balance, and snowmelt. Direct numerical comparison with global model forcing estimates is nevertheless not one-to-one, because the background climate, deposition fields, snow BC treatment, and response metrics differ among studies.

The atmospheric and cloud adjustments diagnosed in this study should be interpreted as secondary responses to the snow-surface perturbation. Their domain-mean magnitude is small, and the present single realization was not designed to quantify a robust cloud-phase feedback. The central result is therefore the directly simulated snow-albedo, surface-radiation, and snowmelt response to prescribed BC deposition. Ensemble experiments with fully interactive aerosol, cloud, and chemistry processes are needed to determine whether the localized cloud changes amplify or damp the deposition-driven surface signal.

Several limitations define the interpretation of the scenario contrasts. First, BC deposition is taken from one Earth system model and therefore does not represent the full uncertainty in future BC emissions, transport, and wet and dry removal. Second, the conversion from prescribed deposition to snow BC loading depends on assumptions about snow accumulation, vertical redistribution, and meltwater scavenging. Third, the common SSP2-4.5 meteorological background intentionally excludes scenario-related changes in circulation, temperature, precipitation, and snow state. The reported values should consequently be interpreted as the

https://doi.org/10.5194/egusphere-2026-4792
Preprint. Discussion started: 4 September 2026

contribution of the BC-deposition pathway, not as the total difference in Arctic climate among the three SSPs.

Within these bounds, the SSP1-2.6 versus SSP5-8.5 contrast provides a quantitative measure of the potential land-surface benefit associated with lower BC deposition by mid-century. A 39.6 % decrease in deposition is accompanied by weaker snow darkening, smaller net-radiation perturbations, and less snowmelt acceleration, although the size of each benefit differs across regions. Future assessments should combine multi-model deposition ensembles, source-resolved BC fields, and scenario-specific climate backgrounds to constrain the full Arctic climate benefit of BC mitigation.

4. Conclusion

This study quantified the Arctic land-surface response to scenario-dependent BC deposition during 2046–2050 using Polar-WRF coupled online with the SNICAR snow-albedo scheme. By applying SSP1-2.6, SSP2-4.5, and SSP5-8.5 BC deposition fields under a common SSP2-4.5 meteorological background, the simulations isolate the contribution of the BC-deposition pathway rather than the full climate response to each SSP.

BC deposition produces substantial, scenario-dependent changes in Arctic snow and surface climate. Under SSP1-2.6, SSP2-4.5, and SSP5-8.5, Arctic-mean spring snow albedo decreases by 16.9 %, 18.1 %, and 19.3 %, respectively. Surface net radiation increases by 1.0–1.4 W m^{-2}, spring snowmelt increases by 4.1–6.1 mm d^{-1}, snow disappearance advances by 6.7–7.6 days, and Arctic-land mean near-surface air temperature increases by 0.09–0.12 °C.

The response is spatially heterogeneous. Greenland has the strongest snow-albedo reduction and snowmelt response despite relatively low BC deposition because its snow cover is deep and persistent. The European Arctic and West Siberia show stronger surface-radiative responses where snow darkening coincides with larger incoming solar radiation, whereas East Siberia shows the weakest overall response. Relative to SSP5-8.5, the 39.6 % lower BC deposition under SSP1-2.6 reduces the BC-induced snow-albedo, net-radiation, and snowmelt responses by 12.4 %, 28.6 %, and 32.8 %, respectively.

These results demonstrate that cleaner mid-century pathways, through lower BC deposition, weaken Arctic snow darkening and spring snowmelt acceleration. The magnitude and geographical expression of this benefit vary across the Arctic, indicating that the climate

https://doi.org/10.5194/egusphere-2026-4792
Preprint. Discussion started: 4 September 2026

implications of BC-deposition changes should be interpreted in the context of regional snow and radiative environments. The quantified effects remain subject to uncertainties in future BC deposition, snow BC parameterization, and the fixed meteorological background. Multi-model deposition ensembles and fully coupled chemistry–climate simulations are needed to quantify the complete climate response. By isolating the BC-deposition pathway, the present analysis provides a process-based, regional reference for assessing the land-surface climate implications of BC mitigation during the mid-21st century.

Author contribution. ZZ and MZ initiated the study and designed the experiments. ZZ performed the simulations and carried out the data analysis. LZ and MZ provided useful comments on the paper. ZZ prepared the manuscript with contributions from all co-authors.

Code availability. The code of Polar-WRF can get from the https://polarmet.osu.edu/PWRF/registration.php, the SNICAR source can download in https://github.com/mflanner/SNICARv3, Polar-WRF/Noah-MP coupled with SNICAR code is available at https://github.com/ZhangZiLu0831/PWRF_NoahMP_SNICAR.

Data availability. The ERA5 reanalysis data were produced by the European Centre for Medium-Range Weather Forecasts (ECMWF) (https://doi.org/10.24381/cds.adbb2d47, Copernicus Climate Change Service, 2023). The snow depth data used the National Centers for Environmental Prediction (NCEP) operational Global Data Assimilation System (GDAS) final analysis data (https://doi.org/10.5065/D6M043C6, National Centersfor Environmental Prediction et al., 2000). The sea ice thickness, snow depth on sea ice, and sea ice albedo data are provided by the National Snow and Ice Data Center (NSIDC;https://doi.org/10.5067/96JO0KIFDAS8, National Snow and Ice Data Center, 2023). The bias-corrected CMIP6 dataset generated using the high-resolution MPI-ESM1-2-HR model output under the SSP2-4.5 scenario were provided from Xu et al. (2021) (https://doi.org/10.11922/sciencedb.00487). The BC deposition fluxes used to prescribe snow BC concentrations are derived from The Earth System Grid Federation (ESGF, https://esgfnode.ipsl.upmc.fr/search/cmip6-ipsl/)

Competing interests. The contact author has declared that noneof the authors has any comp eting interests.

https://doi.org/10.5194/egusphere-2026-4792
Preprint. Discussion started: 4 September 2026

Acknowledgements. The simulations conducted in this studywere supported by the National Key Scientific and Technological Infrastructure project “Earth System Numerical Simulation Fa cility” (Earth Lab).

References

Bokhorst, S., Pedersen, S. H., Brucker, L., Anisimov, O., Bjerke, J. W., Brown, R. D., Ehrich, D., Essery, R. L., Heilig, A., Ingvander, S., Johansson, C., Johansson, M., Jonsdottir, I. S., Inga, N., Luojus, K., Macelloni, G., Mariash, H., McLennan, D., Rosqvist, G. N., Sato, A., Savela, H., Schneebeli, M., Sokolov, A., Sokratov, S. A., Terzago, S., Vikhamar-Schuler, D., Williamson, S., Qiu, Y., and Callaghan, T. V.: Changing Arctic snow cover: A review of recent developments and assessment of future needs for observations, modelling, and impacts, Ambio, 45, 516-537, 10.1007/s13280-016-0770-0, 2016.

Chapin, F. S., Sturm, M., Serreze, M. C., McFadden, J. P., Key, J. R., Lloyd, A. H., McGuire, A. D., Rupp, T. S., Lynch, A. H., Schimel, J. P., Beringer, J., Chapman, W. L., Epstein, H. E., Euskirchen, E. S., Hinzman, L. D., Jia, G., Ping, C.-L., Tape, K. D., Thompson, C. D. C., Walker, D. A., and Welker, J. M.: Role of Land-Surface Changes in Arctic Summer Warming, Science, 310, 657-660, doi:10.1126/science.1117368, 2005.

Chen, Y., Xing, Y., Yan, S., Hou, Y., Li, X., Shi, T., Cui, J., Wu, D., Zhou, Y., Hao, D., Pu, W., and Wang, X.: A Comprehensive Evaluation of Black Carbon in Snow and Its Radiative Forcing in CMIP5 and CMIP6 Models Based on Global Field Observations, Journal of Geophysical Research: Atmospheres, 129, e2023JD040665, https://doi.org/10.1029/2023JD040665, 2024.

Dou, T.-F. and Xiao, C.-D.: An overview of black carbon deposition and its radiative forcing over the Arctic, Advances in Climate Change Research, 7, 115-122, 10.1016/j.accre.2016.10.003, 2016.

Flanner, M. G., Zender, C. S., Randerson, J. T., and Rasch, P. J.: Present-day climate forcing and response from black carbon in snow, Journal of Geophysical Research, 112, 10.1029/2006jd008003, 2007.

https://doi.org/10.5194/egusphere-2026-4792
Preprint. Discussion started: 4 September 2026

Flanner, M. G., Arnheim, J. B., Cook, J. M., Dang, C., He, C., Huang, X., Singh, D., Skiles, S. M., Whicker, C. A., and Zender, C. S.: SNICAR-ADv3: a community tool for modeling spectral snow albedo, Geoscientific Model Development, 14, 7673-7704, 10.5194/gmd-14-7673-2021, 2021.

Hao, D., Bisht, G., Wang, H., Xu, D., Huang, H., Qian, Y., and Leung, L. R.: A cleaner snow future mitigates Northern Hemisphere snowpack loss from warming, Nature Communications, 14, 6074, 10.1038/s41467-023-41732-6, 2023.

Hines, K. M. and Bromwich, D. H.: Development and Testing of Polar Weather Research and Forecasting (WRF) Model. Part I: Greenland Ice Sheet Meteorology, Monthly Weather Review, 136, 1971-1989, 10.1175/2007MWR2112.1, 2008.

Hines, K. M., Bromwich, D. H., Bai, L., Bitz, C. M., Powers, J. G., and Manning, K. W.: Sea Ice Enhancements to Polar WRF, Monthly Weather Review, 143, 2363-2385, 10.1175/MWR-D-14-00344.1, 2015.

Hines, K. M., Bromwich, D. H., Wang, S. H., Silber, I., Verlinde, J., and Lubin, D.: Microphysics of summer clouds in central West Antarctica simulated by the Polar Weather Research and Forecasting Model (WRF) and the Antarctic Mesoscale Prediction System (AMPS), Atmos. Chem. Phys., 19, 12431-12454, 10.5194/acp-19-12431-2019, 2019.

Iacono, M. J., Delamere, J. S., Mlawer, E. J., Shephard, M. W., Clough, S. A., and Collins, W. D.: Radiative forcing by long-lived greenhouse gases: Calculations with the AER radiative transfer models, Journal of Geophysical Research: Atmospheres, 113, 10.1029/2008JD009944, 2008.

Jiao, C., Flanner, M. G., Balkanski, Y., Bauer, S. E., Bellouin, N., Berntsen, T. K., Bian, H., Carslaw, K. S., Chin, M., De Luca, N., Diehl, T., Ghan, S. J., Iversen, T., Kirkevåg, A., Koch, D., Liu, X., Mann, G. W., Penner, J. E., Pitari, G., Schulz, M., Seland, Ø., Skeie, R. B., Steenrod, S. D., Stier, P., Takemura, T., Tsigaridis, K., van Noije, T., Yun, Y., and Zhang, K.: An AeroCom assessment of black carbon in Arctic snow and sea ice, Atmospheric Chemistry and Physics, 14, 2399-2417, 10.5194/acp-14-2399-2014, 2014.

Kain, J. S.: The Kain–Fritsch Convective Parameterization: An Update, Journal of Applied Meteorology, 43, 170-181, https://doi.org/10.1175/1520-0450(2004)043<0170:TKCPAU>2.0.CO;2, 2004.

Kühn, T., Kupiainen, K., Miinalainen, T., Kokkola, H., Paunu, V.-V., Laakso, A., Tonttila, J., Van Dingenen, R., Kulovesi, K., Karvosenoja, N., and Lehtinen, K. E. J.: Effects of black carbon mitigation on Arctic climate, Atmospheric Chemistry and Physics, 20, 5527-5546, 10.5194/acp-20-5527-2020, 2020a.

Kühn, T., Kupiainen, K., Miinalainen, T., Kokkola, H., Paunu, V. V., Laakso, A., Tonttila, J., Van Dingenen, R., Kulovesi, K., Karvosenoja, N., and Lehtinen, K. E. J.: Effects of black carbon mitigation on Arctic climate, Atmos. Chem. Phys., 20, 5527-5546, 10.5194/acp-20-5527-2020, 2020b.

Morrison, H. and Gettelman, A.: A New Two-Moment Bulk Stratiform Cloud Microphysics Scheme in the Community Atmosphere Model, Version 3 (CAM3). Part I: Description and Numerical Tests, Journal of Climate, 21, 3642-3659, 10.1175/2008JCLI2105.1, 2008.

Nakanishi, M. and Niino, H.: An Improved Mellor–Yamada Level-3 Model: Its Numerical Stability and Application to a Regional Prediction of Advection Fog, Boundary-Layer Meteorology, 119, 397-407, 10.1007/s10546-005-9030-8, 2006.

Nakanishi, M. and Niino, H.: Development of an Improved Turbulence Closure Model for the Atmospheric Boundary Layer, Journal of the Meteorological Society of Japan. Ser. II, 87, 895-912, 10.2151/jmsj.87.895, 2009.

Niu, G.-Y., Yang, Z.-L., Mitchell, K. E., Chen, F., Ek, M. B., Barlage, M., Kumar, A., Manning, K., Niyogi, D., Rosero, E., Tewari, M., and Xia, Y.: The community Noah land surface model with multiparameterization options (Noah-MP): 1. Model description and evaluation with local-scale measurements, Journal of Geophysical Research: Atmospheres, 116, 10.1029/2010JD015139, 2011.

O'Neill, B. C., Kriegler, E., Riahi, K., Ebi, K. L., Hallegatte, S., Carter, T. R., Mathur, R., and van Vuuren, D. P.: A new scenario framework for climate change research: the concept of shared socioeconomic pathways, Climatic Change, 122, 387-400, 10.1007/s10584-013-0905-2, 2014.

Qi, L. and Wang, S.: Sources of black carbon in the atmosphere and in snow in the Arctic, Science of The Total Environment, 691, 442-454, 10.1016/j.scitotenv.2019.07.073, 2019.

Rantanen, M., Karpechko, A. Y., Lipponen, A., Nordling, K., Hyvärinen, O., Ruosteenoja, K., Vihma, T., and Laaksonen, A.: The Arctic has warmed nearly four times faster than the globe since 1979, Communications Earth & Environment, 3, 168, 10.1038/s43247-022-00498-3, 2022.

https://doi.org/10.5194/egusphere-2026-4792
Preprint. Discussion started: 4 September 2026

Riahi, K., van Vuuren, D. P., Kriegler, E., Edmonds, J., O'Neill, B. C., Fujimori, S., Bauer, N., Calvin, K., Dellink, R., Fricko, O., Lutz, W., Popp, A., Cuaresma, J. C., Kc, S., Leimbach, M., Jiang, L., Kram, T., Rao, S., Emmerling, J., Ebi, K., Hasegawa, T., Havlik, P., Humpenöder, F., Da Silva, L. A., Smith, S., Stehfest, E., Bosetti, V., Eom, J., Gernaat, D., Masui, T., Rogelj, J., Strefler, J., Drouet, L., Krey, V., Luderer, G., Harmsen, M., Takahashi, K., Baumstark, L., Doelman, J. C., Kainuma, M., Klimont, Z., Marangoni, G., Lotze-Campen, H., Obersteiner, M., Tabeau, A., and Tavoni, M.: The Shared Socioeconomic Pathways and their energy, land use, and greenhouse gas emissions implications: An overview, Global Environmental Change, 42, 153-168, https://doi.org/10.1016/j.gloenvcha.2016.05.009, 2017.

Sand, M., Berntsen, T. K., von Salzen, K., Flanner, M. G., Langner, J., and Victor, D. G.: Response of Arctic temperature to changes in emissions of short-lived climate forcers, Nature Climate Change, 6, 286-289, 10.1038/nclimate2880, 2016.

Toon, O. B., McKay, C. P., Ackerman, T. P., and Santhanam, K.: Rapid calculation of radiative heating rates and photodissociation rates in inhomogeneous multiple scattering atmospheres, Journal of Geophysical Research: Atmospheres, 94, 16287-16301, 10.1029/JD094iD13p16287, 1989.

von Salzen, K., Whaley, C. H., Anenberg, S. C., Van Dingenen, R., Klimont, Z., Flanner, M. G., Mahmood, R., Arnold, S. R., Beagley, S., Chien, R.-Y., Christensen, J. H., Eckhardt, S., Ekman, A. M. L., Evangeliou, N., Faluvegi, G., Fu, J. S., Gauss, M., Gong, W., Hjorth, J. L., Im, U., Krishnan, S., Kupiainen, K., Kühn, T., Langner, J., Law, K. S., Marelle, L., Olivié, D., Onishi, T., Oshima, N., Paunu, V.-V., Peng, Y., Plummer, D., Pozzoli, L., Rao, S., Raut, J.-C., Sand, M., Schmale, J., Sigmond, M., Thomas, M. A., Tsigaridis, K., Tsyro, S., Turnock, S. T., Wang, M., and Winter, B.: Clean air policies are key for successfully mitigating Arctic warming, Communications Earth & Environment, 3, 222, 10.1038/s43247-022-00555-x, 2022.

Xu, Z., Han, Y., Tam, C.-Y., Yang, Z.-L., and Fu, C.: Bias-corrected CMIP6 global dataset for dynamical downscaling of the historical and future climate (1979–2100), Scientific Data, 8, 293, 10.1038/s41597-021-01079-3, 2021.

Zhang, Z., Zhou, L., and Zhang, M.: A progress review of black carbon deposition on Arctic snow and ice and its impact on climate change, Advances in Polar Science, 35, 178-191, 10.12429/j.advps.2023.0024, 2024.

https://doi.org/10.5194/egusphere-2026-4792
Preprint. Discussion started: 4 September 2026

Zhang, Z., Zhou, L., and Zhang, M.: A numerical sensitivity study on the snow-darkening effect by black carbon deposition over the Arctic in spring, Atmos. Chem. Phys., 25, 1-25, 10.5194/acp-25-1-2025, 2025.

Zhang, Z., Zhou, L., Zhang, M., Ma, S., Li, F., and Zhu, J.: Modeling and analysis of winter arctic clouds and their radiative impacts using three microphysics schemes in polar-WRF, Atmospheric Research, 340, 109059, https://doi.org/10.1016/j.atmosres.2026.109059, 2026.